Cellular/Molecular

Reproducibility of the Rod Photoreceptor Response Depends Critically on the Concentration of the Phosphodiesterase Effector Enzyme

Ala Morshedian,[1] Gabriela Sendek,[1] Sze Yin Ng,[1] Kimberly Boyd,[2] Roxana A. Radu,[1] Mingyao Liu,[3] Nikolai O. Artemyev,[2] Alapakkam P. Sampath,[1] and Gordon L. Fain[1,4]

[1]Stein Eye Institute, David Geffen School of Medicine, University of California Los Angeles, Los Angeles, California, 90095-7000, [2]Department of Molecular Physiology and Biophysics, University of Iowa, Iowa City, Iowa, 52242, [3]Shanghai Key Laboratory of Regulatory Biology, Institute of Biomedical Sciences and School of Life Sciences, East China Normal University, Shanghai, China, 200062, and [4]Department of Integrative Biology and Physiology, University of California Los Angeles, Los Angeles, California 90095-7239

The high sensitivity of night vision requires that rod photoreceptors reliably and reproducibly signal the absorption of single photons, a process that depends on tight regulation of intracellular cGMP concentration through the phototransduction cascade. Here in the mouse (Mus musculus), we studied a single-site *D167A* mutation of the gene for the α subunit of rod photoreceptor phosphodiesterase (PDEA), made with the aim of removing a noncatalytic binding site for cGMP. This mutation unexpectedly eliminated nearly all PDEA expression and reduced expression of the β subunit (PDEB) to ~5%-10% of WT. The remaining PDE had nearly normal specific activity; degeneration was slow, with 50%-60% of rods remaining after 6 months. Responses were larger and more sensitive than normal but slower in rise and decay, probably from slower dark turnover of cGMP. Remarkably, responses became much less reproducible than WT, with response variance increasing for amplitude by over 10-fold, and for latency and time-to-peak by >100-fold. We hypothesize that the increase in variance is the result of greater variability in the dark-resting concentration of cGMP, produced by spatial and temporal nonuniformity in spontaneous PDE activity. This variability decreased as stimuli were made brighter, presumably because of greater spatial uniformity of phototransduction and the approach to saturation. We conclude that the constancy of the rod response depends critically on PDE expression to maintain adequate spontaneous PDE activity, so that the concentration of second messenger is relatively uniform throughout the outer segment.

Key words: GAF A domain; phosphodiesterase; rod photoreceptor; sensitivity; single-photon response; transduction

Significance Statement

Rod photoreceptors in the vertebrate retina reliably signal the absorption of single photons of light by generating responses that are remarkably reproducible in amplitude and waveform. We show that this reproducibility depends critically on the concentration of the effector enzyme phosphodiesterase (PDE), which metabolizes the second messenger cGMP and generates rod light responses. In rods with the *D167A* mutation of the α subunit of PDE, only 5%-10% of PDE is expressed. Single-photon responses then become much more variable than in WT rods. We think this variability is caused by spatial and temporal inhomogeneity in the concentration of cGMP in darkness, so that photons absorbed in different parts of the cell produce responses of greatly varying amplitude and waveform.

Received Oct. 22, 2021; revised Dec. 11, 2021; accepted Dec. 29, 2021.

Author contributions: A.M., N.O.A, R.A.R., M.L., A.P.S. and G.L.F. designed research; A.M., G.S., S.Y.N., K.B., and M.L. performed research; A.M., G.S., S.Y.N., K.B., N.O.A., and G.L.F. analyzed data; A.M., N.O.A., A.P.S., and G.L.F. edited the paper; A.M., N.O.A., R.A.R., and G.L.F. wrote the paper.

This work was supported by National Eye Institute, National Institutes of Health Grants EY001844 to G.L.F., EY29817 to A.P.S., EY010843 to N.O.A., and EY025002 to R.A.R.; Research to Prevent Blindness USA unrestricted grant to the UCLA Department of Ophthalmology; and National Eye Institute Core Grant EY00311 to the Stein Eye Institute. We thank Ekaterina Bikovtseva, Jane Hu Coffman, and Chunni Zhu for technical assistance; and Ching-Kang (Jason) Chen for help in the initial stages of this investigation.

The authors declare no competing financial interests.

Correspondence should be addressed to Gordon L. Fain at gfain@ucla.edu.

https://doi.org/10.1523/JNEUROSCI.2119-21.2021

Introduction

The response of a rod photoreceptor is produced by a G-protein cascade: absorption of light by rhodopsin activates the G-protein transducin, which in turn binds to and stimulates a phosphodiesterase effector protein (PDE) to hydrolyze the second messenger guanosine 3′,5′-cyclic monophosphate (cGMP) (Burns and Pugh, 2010; Arshavsky and Burns, 2012; Reingruber et al., 2015; Fain, 2019). Rod PDE is an unusual member of the PDE family, consisting of two different catalytic α and β subunits (PDEA and PDEB) and two identical regulatory γ subunits (PDEG). The PDEG bind activated transducin and control the activity of

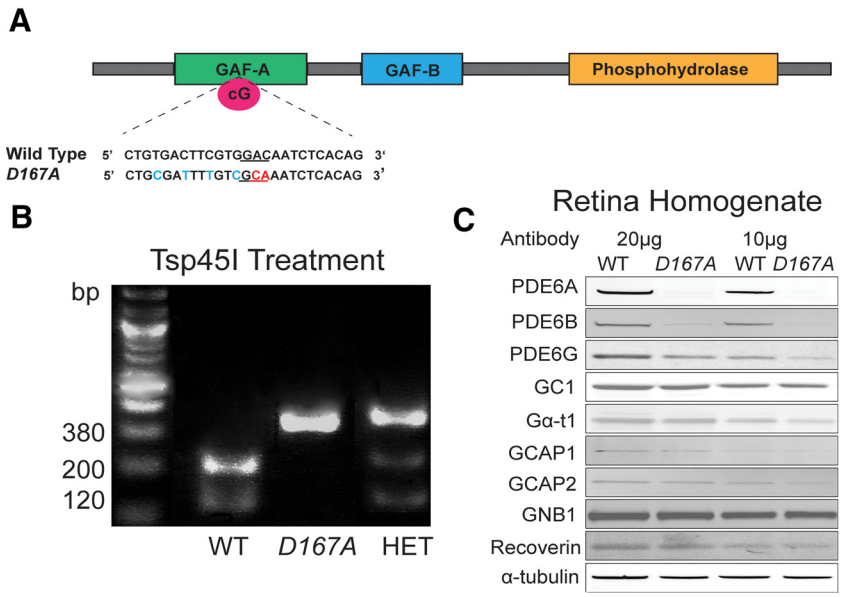

Figure 1. Generation of $PDEA^{D167A/D167A}$ mice. ***A***, Schematic showing *D167A* mutation site located within the GAF A cyclic-nucleotide-binding domain of *PDEA*. Blue indicates nucleotide changes producing no change in amino-acid sequence; red are changes altering aspartate to alanine. ***B***, The mutation removes a cleavage site recognized by Tsp45I. *D167A* is band for $PDEA^{D167A/D167A}$; *HET* is heterozygote (i.e., $PDEA^{D167A/+}$). ***C***, Representative immunoblots of phototransduction proteins with 20 and 10 µg of retinal homogenates from 3-month-old WT and $PDEA^{D167A/D167A}$ mutant mice. After normalization to α-tubulin, PDEA and PDEB levels were significantly lower in $PDEA^{D167A/D167A}$, while other phototransduction proteins were little affected.

the PDE catalytic subunits (Cote, 2021; Gulati and Palczewski, 2021). In addition to their catalytic binding sites, each of the PDEA and PDEB subunits has two GAF domains, of which one (GAF A) has been shown to encode a noncatalytic binding site for cGMP. GAF domains in other PDE families can regulate PDE activity, but the function of the noncatalytic binding site for cGMP in photoreceptor PDE has long been disputed and remains unclear (see, e.g., Cote et al., 1994; Calvert et al., 1998; Cote, 2021).

Binding of cGMP to the GAF A region of PDE can be significantly reduced by removal of a key aspartate residue (Muradov et al., 2004). We therefore made a mouse line in which rod PDEA had a *D167A* mutation to remove this aspartate, with the hope of testing the role of noncatalytic cGMP binding in rod function. Much to our surprise, this mutation nearly eliminated expression of *PDEA* and reduced *PDEB* expression to only ~5%-10% of WT. PDE activity was reduced in *D167A* retinas in approximate proportion to the reduction in *PDEB* expression, indicating that the PDE remaining in $PDEA^{D167A/D167A}$ retinas had nearly normal specific activity. Rods had robust light responses larger and more sensitive than WT rods, but response waveforms were much slower in decay, probably from a decrease in dark cGMP turnover. The most striking effect was a marked increase in the variance of response amplitude, latency, and time to peak, particularly evident at dim light intensities. The most likely explanation of this effect is that the decrease in PDE concentration produced a decrease in spontaneous PDE activity. In consequence, there was greater spatial and temporal variability in the outer-segment cGMP concentration in darkness, resulting in greater variation in the effect of single photons absorbed in different places in the outer segment (Reingruber et al., 2013). Our observations show that the concentration of PDE in the disk membrane of a rod is critical in determining both the kinetics of the rod response and its reproducibility.

Materials and Methods

Mice and genotyping. To make mice with the *PDEA D167A* mutation, C57BL/6J mice were purchased from the Shanghai Laboratory Animal Center, CAS. Mouse one-cell embryos were obtained by superovulation of females mated with males having the same genetic background. The embryos were harvested in M2 medium (Sigma-Aldrich) and cultured in KSOM embryo medium (Sigma-Aldrich) for 2-3 h. Knock-in was performed by microinjection of Tris-EDTA buffer solution (Thermo Fisher Scientific) containing 12.5 ng/µl sgRNA (5′-TGAGCATTT CTGTGACTTCG), 50 ng/µl donor DNA (5′-TCTGTCTCTCTGTCCTTGACTCTTTCAGGAT GAGCATTTCTGCGATTTGTCGCAAATCTCAC-AGAATATCAGACCAAAAACATCCTGGCTTC-CCCCAT), and 30 nM Cas9 protein (Thermo Fisher Scientific) into the pronuclei of one-cell-stage embryos according to previously described methods (Wang et al., 2015). Injected embryos were transferred into pseudo-pregnant female mice immediately after injection or the next morning after overnight culture in KSOM medium. All experiments were performed in accordance with the regulations of the Association for Assessment and Accreditation of Laboratory Animal Care in Shanghai and were approved by the East China Normal University Center for Animal Research (AR2013/04009). After the animals were made, they were transferred to the University of California, Los Angeles.

Biochemical and electrophysiological experiments were performed on C57BL/6J WT mice (The Jackson Laboratory) and $PDEA^{D167A/D167A}$ mice in accordance with the policy of *The Journal of Neuroscience*, as well as with the rules and regulations of the National Institutes of Health guidelines for research animals as approved by the institutional animal care and use committees of the University of California, Los Angeles, and of the University of Iowa (Iowa City, Iowa). Animals were kept under a 12:12 h light/dark cycle in approved cages and supplied with ample food and water. To distinguish between WT and $PDEA^{D167A/D167A}$ animals, we used the following primers: 5′-TGGATGCTGGAGGTGTA CGTGGTCGCCTCA and 5′-ATAGCAAGGTTGGAGAATTCCGT GAACTGG. We subjected 10 µl of the PCR product to 0.5 µl of the Tsp45I endonuclease (New England Biolabs) at 65°C for 1 h. The WT allele yielded bands at 120 and 200 bp, but the disrupted allele generated a 380 bp product (see Fig. 1*B*).

Immunoblotting. Neural-retina tissue from each animal (WT or $PDEA^{D167A/D167A}$) was homogenized in 1× PBS solution with Halt protease inhibitor mixture (Invitrogen). Protein samples were treated with benzonase nuclease (Sigma-Aldrich) at room temperature for 1 h and then rehomogenized with 1% SDS in PBS. Cellular debris was removed by centrifugation (20,000 × *g*, 2 min, 4°C), and protein concentration was determined with the Micro BCA Protein Assay Kit (Thermo Fisher Scientific). We then ran 5-20 µg of total protein from WT or $PDEA^{D167A/D167A}$ retinas on 4%-12% or 12% SDS-PAGE gels (Novex, Thermo Fisher Scientific; Invitrogen). Membranes were blocked with Odyssey Blocking Buffer (LI-COR Biosciences) followed by incubation at room temperature, and they were then probed with primary antibodies at a final dilution of 1 µg/ml. Antibodies were as follows: PDEA (PA1-770, Thermo Fisher Scientific), PDEB (PA1-772, Thermo Fisher Scientific), PDEC (Bio-Synthesis), PDEG (PA1-773,Thermo Fisher Scientific), Ros-GC1 (sc-376217, Santa Cruz Biotechnology), transducin α (Gα-t1, sc-136143, Santa Cruz Biotechnology), GCAP1 (sc-136313, Santa Cruz Biotechnology), GCAP2 (sc-166056, Santa Cruz Biotechnology), transducin β subunit (GNB1, NB120-3433, Novus Biologicals), Recoverin (ab31928, Abcam), and α-tubulin (T9026, Sigma-Aldrich). Western blot analysis was performed with cognate IR dye-labeled secondary antibodies at a dilution of 1:50,000 and detected with an Odyssey CLx Infrared Imaging System (LI-COR).

Assays of PDE activity and inhibition by PDEγ. For each genotype, four mouse retinas were homogenized by sonication (two 5 s pulses) in 220 µl of 20 mM Tris-HCl buffer, pH 7.5, containing 120 mM NaCl, 1 mM $MgSO_4$, and 1 mM mercaptoethanol. After brief centrifugation (20,000 × *g*, 2 min, 4°C) to remove cell debris, retinal homogenates (typically, 5-6 mg protein/ml) were used to measure basal PDE activities with final dilutions of 1:140 for WT retinas and 1:24 for $PDEA^{D167A/D167A}$ retinas. Maximal (trypsin-activated) PDE activities were measured from retinal homogenates treated with trypsin (100 mg/ml) for 10 min at 25°C. Trypsin treatment was terminated by the addition of 10× soybean trypsin inhibitor (Sigma) and incubation for 5 min at 25°C, followed by centrifugation at 20,000 × *g* for 3 min at 4°C. The final dilutions of trypsin-treated retinal homogenates in the assays of maximal PDE activity were 1:4000 for WT retinas and 1:400 for $PDEA^{D167A/D167A}$ retinas. PDE assays were conducted in 40 µl of 20 mM Tris-HCl buffer, pH 7.5, containing 120 mM NaCl, 2 mM $MgSO_4$, 1 mM 2-mercaptoethanol, 0.1 units of bacterial alkaline phosphatase, and 10 μM [^{3}H]cGMP (100,000 counts per minute) for 10-15 min at 25°C. The reaction was terminated by the addition of AG1-X2 cation exchange resin (0.5 ml of 20% bed volume suspension, Bio-Rad). Samples were incubated for 6 min at 25°C with occasional mixing and spun at 10,000 × *g* for 3 min. Then 0.25 ml of the supernatant was removed for counting in a scintillation counter.

Retinal anatomy. Mice were anesthetized with isoflurane and fixed by intracardiac perfusion with 2% formaldehyde and 2.5% glutaraldehyde in 0.1 M sodium phosphate buffer (PB). The superior part of the eye was marked with a light cautery before enucleation. The eyecup was trimmed into hemispheres. All tissues were postfixed with 1% osmium tetroxide in 0.1 M sodium PB followed by dehydration in a graded series of alcohols. The hemispheres were embedded in Epon resin. Semithin sections (1 µm) were cut along the entire eye hemisphere from superior to inferior, passing through the optic nerve head. Sections were stained with 0.5% toluidine blue and 1% sodium borate. For the "spider" plot of Figure 3*B*, images of the whole hemisphere were obtained from an Olympus confocal microscope (FV-1000) with the multi-time-lapse function under a 40× oil-immersion objective. The thickness of the outer nuclei layer was measured in 200 µm intervals from the optic nerve head with ImageJ software. The average thickness of the outer nuclei layer was obtained from 9 to 11 sections in 3 mice per genotype. Light micrographs were photographed with a Zeiss Axiophot microscope equipped with a 40× oil-immersion objective and a CoolSNAP digital camera (Photometrics).

Suction-electrode recording. Mice were dark-adapted overnight and killed before tissue extraction by cervical dislocation. All animals used for recording were younger than 6 months and were selected indiscriminately from either sex. Eyes were enucleated under dim red light. The anterior portion of the eye was cut, and the lens and cornea were removed in darkness by means of infrared image converters. The retina was isolated from the eyecup; the retinal pigment epithelium was removed with fine tweezers, and the retina was chopped into small pieces with a razor blade. The pieces were then transferred to the recording chamber in complete darkness by means of infrared goggles (American Technologies Network).

Responses of single photoreceptor outer segments were recorded at 35°C-38°C with the suction-electrode technique (Baylor et al., 1979). The change in outer-segment membrane current produced by a stimulus was recorded with a current-to-voltage converter (Axopatch 200A, Molecular Devices), low-pass filtered at 30 Hz with an eight-pole Bessel filter (Kemo Limited Electronic Filters), and sampled at 100 Hz. Digitized data were recorded with Clampex, version 8.0 (Molecular Devices), and were analyzed with Origin Pro (OriginLab). Curve fitting and plotting of data were also performed in Origin Pro. Calculations of mean and variance were conducted either in Origin Pro or in Excel (Microsoft); values are given as the mean ± SEM unless otherwise stated. Statistical tests were performed with MATLAB (see below).

During recording, the photoreceptors were continuously perfused with Ames' medium (Sigma), containing an additional 1.9 g/l $NaHCO_3$ and equilibrated with 95% O_2/5% CO_2. The osmolarity of the medium was measured with a vapor-pressure osmometer (Wescor) and was then adjusted to 284 mOsm. Temperature was maintained at 35°C-38°C with an automatic temperature controller (Warner Instruments). The recording electrodes were filled with Locke's solution, which contained the following (in mM): 93 NaCl, 2.1 KCl, 2.6 $CaCl_2$, 1.8 $MgCl_2$, 2.0 $NaHCO_3$, and 10.8 HEPES buffer, pH 7.4. Fire-polished borosilicate glass was pulled with a micropipette puller (P-97; Sutter Instruments) to produce pipettes with rapidly tapering shanks used for recordings. The tip size was further adjusted under a compound microscope by moving the pipette close to a platinum heating wire until the tip had melted to an inner diameter that would fit the outer segment of the photoreceptor and provide a good seal.

Illumination was delivered with an OptoLED optical system (Cairn Research) coupled to an inverted microscope. We used a 505 nm monochromatic LED nearly at the peak of spectral sensitivity of mouse rods (Nymark et al., 2012). The intensity of the light was controlled by the voltage output of the computer to the OptoLED optical system and was calibrated with a photodiode (OSI Optoelectronics). To estimate the effective collecting area, we gave a series of flashes to both WT and $PDEA^{D167A/D167A}$ rods of 2 photons µm^{-2} (see Fig. 5). For 7 WT rods, we registered 711 nulls out of 1350 flashes, for a probability of failure of 0.53 ± 0.03. From the Poisson equation (see Eq. 2, below), we calculate that flashes bleached an average of 0.63 Rh*, for a collecting area of 0.32 µm^2. With the same light stimuli for 6 $PDEA^{D167A/D167A}$ rods, we registered 619 failures in 1100 flashes, for a probability of failure of 0.56 ± 0.02. The Poisson equation then gave an average number of Rh* per flash as 0.58, for a collecting area of 0.29 µm^2. Because these values of collecting area were similar and not significantly different, we have used a collecting area of 0.3 µm^2 in the remainder of the paper.

Statistical tests. Means were compared with the nonparametric Wilcoxon test in MATLAB, equivalent to a Mann–Whitney *U* test. Bootstrapping was also done in MATLAB with the functions *bootstrp* and *bootci* (for 95% confidence intervals).

Results

In an attempt to investigate the function of noncatalytic binding of cGMP to PDE, we genetically engineered a mouse without a key aspartate in the GAF A domain of PDEA (Fig. 1*A*). We used CRISPR/Cas to replace the GAC codon of aspartate with the GCA codon of alanine, with the hope that removal of the GAF A aspartate would decrease cGMP binding (Muradov et al., 2004). Treatment with the Tsp45I endonuclease verified that $PDEA^{D167A/D167A}$ retinas had only the *D167A* mutant *PDEA* (Fig. 1*B*). When we then examined expression of PDE with Western blots (Fig. 1*C*), we discovered to our surprise that this mutation nearly eliminated PDEA expression and greatly decreased PDEB expression, while leaving the levels of PDEG and other transduction proteins little altered.

PDE expression and activity in $PDEA^{D167A/D167A}$ retinas

To provide a better estimate of the changes in PDE subunit expression, we ran gels with different amounts of protein as in Figure 1*C*. In Figure 2*A*, we show the results of these experiments. Each data point gives the optical density of the PDE protein band normalized to that of the band for tubulin, averaged for the different protein concentrations used in the experiment. The horizontal and vertical lines indicate the global means and SDs for each of the experiments. These results indicate that *PDEA* expression was reduced by >2 orders of magnitude. In retrospect, this result might have been expected, given the importance of the GAF domains in PDE protein folding (Heikaus et al., 2009; Cote et al., 2021). PDEB expression was also significantly reduced to ~5%-10% that of WT rods. No significant change was observed in PDEG expression. In control experiments (not shown), the expression of PDEC (cone PDE) was measured as previously described (Majumder et al., 2015), in quantitative gels like those of Figure 1*C*. We could detect no difference in

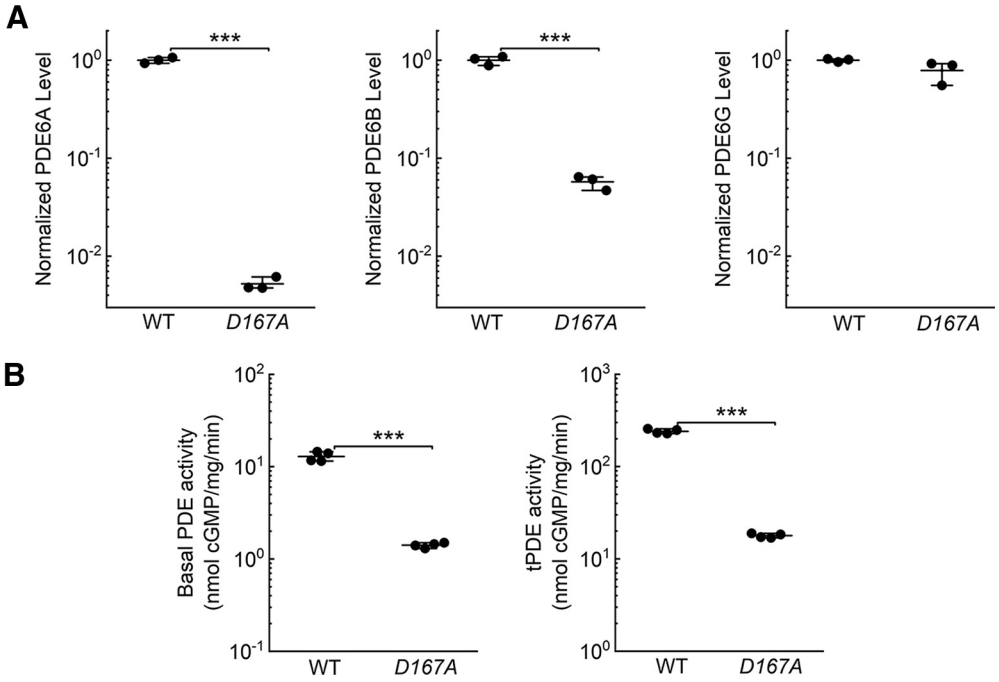

Figure 2. *PDEA*$^{D167A/D167A}$ mutants show reduced PDE expression and activity. Scatterplots represent individual data points from independent experiments together with mean and SD. ***A***, PDEA, PDEB, and PDEG levels in WT compared with *PDEA*$^{D167A/D167A}$ in retinal homogenates. Both PDEA (0.0052 ± 0.0001) and PDEB (0.057 ± 0.007) had a significant reduction in expression ($p = 0.0006$ for PDEA, $p = 0.002$ for PDEB). Although PDEG (0.78 ± 0.1) had a slight reduction in expression, this difference was not statistically different from WT ($p = 0.07$). ***B***, Both basal PDE activity and trypsin-activated PDE activity were reduced in *PDEA*$^{D167A/D167A}$ animals. Basal activity decreased from 12.9 ± 1.5 nmol cGMP/mg/min in WT to 1.4 ± 0.08 nmol cGMP/mg/min in *PDEA*$^{D167A/D167A}$, a factor of ~9 ($n = 4$, $p = 0.0003$). The decrease in total (trypsin-activated) PDE activity was even greater, from 241 ± 13 nmol cGMP/mg/min in WT to 17 ± 0.9 nmol cGMP/mg/min in *PDEA*$^{D167A/D167A}$ ($n = 4$, $p = 0.00002$) or ~14-fold.

the amount of PDEC between WT and *PDEA*$^{D167A/D167A}$ retinas, indicating that *PDEC* was not upregulated in the mutant rods.

In Figure 2*B*, we compare basal PDE activity (left) and trypsin-activated activity (right) measured from WT and *PDEA*$^{D167A/D167A}$ retinas. Limited treatment with trypsin cleaves and removes the PDEG subunit from the holoenzyme, providing an estimate of the maximal value of enzymatic activity (Baehr et al., 1979). These measurements show that basal and trypsin-activated activities are reduced by factors of ~9 and ~14 in *PDEA*$^{D167A/D167A}$ rods. The reduction in rod activity is likely to be somewhat greater because cones would be expected to contribute 1%-2% of PDE activity in both WT and mutant mice.

Because the decrease in enzyme activity in Figure 2*B* is similar to the decrease in protein expression in Figure 2*A*, our measurements indicate that the PDE expressed in *PDEA*$^{D167A/D167A}$ rods has about the same specific activity as the PDE holoenzyme in WT rods. Most of this activity in mutant retinas is probably produced by PDEB dimers because of the importance of dimeric structure for PDE enzyme function (see Cote, 2021; Gulati and Palczewski, 2021). We were, however, unable to make any physical measurements of enzyme properties from the small amount of PDE available from the *PDEA*$^{D167A/D167A}$ mice.

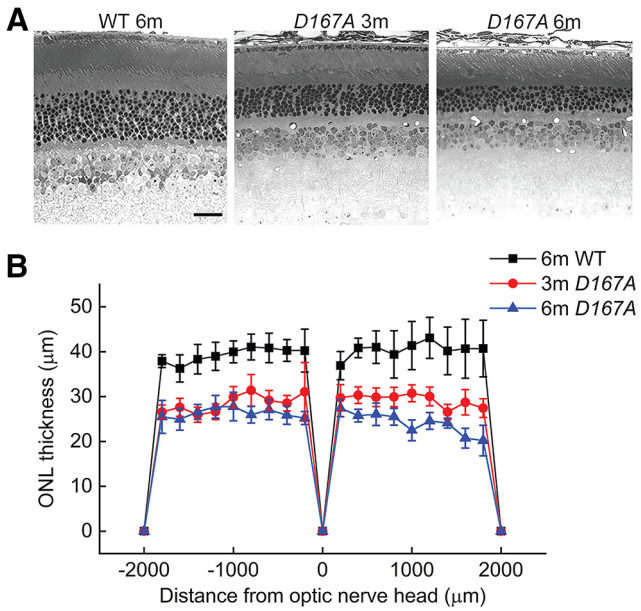

Figure 3. Comparison of anatomy and degeneration of WT and *PDEA*$^{D167A/D167A}$ retinas. ***A***, Representative cross sections of the retina. Left, 6 month-old WT. Middle, 3-month-old *PDEA*$^{D167A/D167A}$ retina. Right, 6-month-old *PDEA*$^{D167A/D167A}$ retina. Scale bar, 20 μm. ***B***, Thickness of the outer nuclei layer (ONL) was measured in 200 μm intervals from the optic nerve head. Plot includes data from 6-month-old WT retinas ($n = 3$), 3-month-old *PDEA*$^{D167A/D167A}$ retinas ($n = 4$), and 6-month-old *PDEA*$^{D167A/D167A}$ retinas ($n = 4$). Data points give means with SEMs.

Anatomy and retinal degeneration

Since a null mutation of *PDEB* produces rapid degeneration of the rods (*rd1*) (Bowes et al., 1990), we asked whether the almost complete absence of PDEA would have a similar effect. In Figure 3, we show the results of a light-microscopic investigation of retinal anatomy comparing WT and mutant mice. Rods in *PDEA*$^{D167A/D167A}$ retinas degenerated very slowly, with >50% of rod nuclei still present even in 6-month-old animals and with no apparent difference between the center and periphery. This result is of considerable interest because it indicates that PDEB largely by itself can preserve rod structure and function, although PDEA by itself cannot. Degeneration in *PDEA*$^{D167A/D167A}$ retinas is much slower than for other reported mouse models with single-

site mutations in *PDEA*, which all produce extensive rod loss within the first month of age (Sakamoto et al., 2009; Sothilingam et al., 2015).

The outer segments of $PDEA^{D167A/D167A}$ rods seemed similar in length to those of WT mice. Moreover, our calculation of collecting areas for WT and $PDEA^{D167A/D167A}$ rods in animals 4-6 weeks of age gave similar values (see Materials and Methods). This correspondence indicates that, at least in young mice, the dimensions of the rods are likely to have been similar. No attempt was made to measure collecting areas or rod length at later ages.

Suction-electrode recording from $PDEA^{D167A/D167A}$ rods

In Figure 4, we show suction-electrode recordings from WT (Fig. 4*A*) and $PDEA^{D167A/D167A}$ rods (Fig. 4*B*) to a series of increasing light intensities. The mean amplitude of the $PDEA^{D167A/D167A}$ rod response was nearly twice that of WT rods. This difference reflects the lower expression level and decreased basal activity of the PDE (Fig. 2), which would produce a greater outer-segment cGMP concentration and a larger dark current. The responses of $PDEA^{D167A/D167A}$ rods were also much slower in decay, as is particularly evident at the dimmer light intensities. Fits of the decaying phases of small-amplitude responses with single exponentials gave mean values of time constants (τ_{REC}) of 140 ± 18 ms for WT rods and 730 ± 120 ms for $PDEA^{D167A/D167A}$ rods. These differences in decay time are largely the result of the low basal activity of the PDE and slower turnover of cGMP in darkness (β_D), in agreement with recent model calculations (Abtout et al., 2021). There may also have been some differences in the function of the PDE itself, since we saw a small difference in the limiting time constant (τ_D) of PDE decay (200 ± 16 ms for WT rods, 280 ± 14 ms for $PDEA^{D167A/D167A}$ rods).

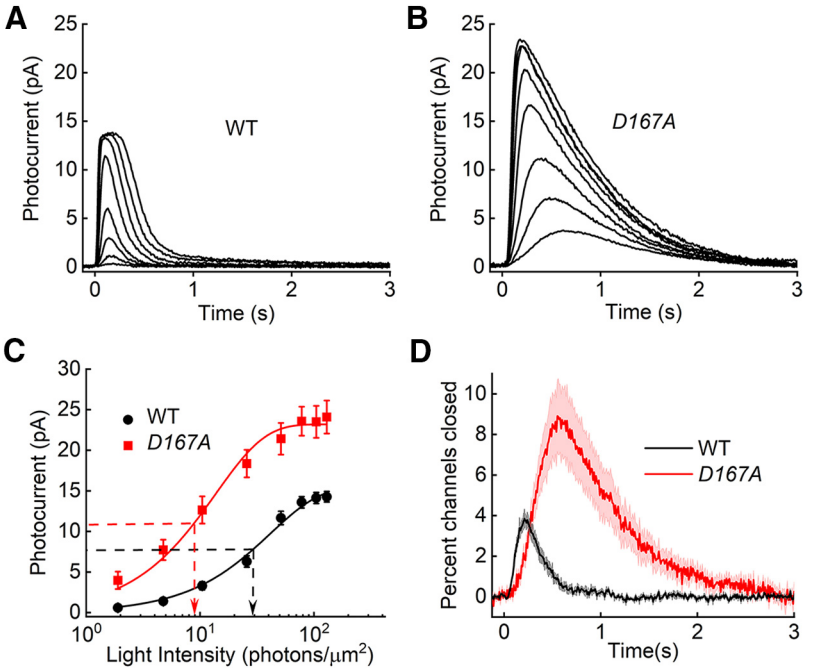

Figure 4. Suction-electrode recordings from $PDEA^{D167A/D167A}$ and WT rods. ***A***, ***B***, Mean responses for stimuli of 1.9, 4.8, 10.5, 25.7, 51.3, 77.9, 105, and 129 photons μm^{-2}. ***A***, WT rods ($n = 10$). ***B***, $PDEA^{D167A/D167A}$ rods ($n = 11$). Peak amplitudes averaged 13.8 ± 0.5 pA for WT and 23.2 ± 2.1 pA for $PDEA^{D167A/D167A}$. ***C***, Response-intensity curves of WT (black circles) and $PDEA^{D167A/D167A}$ (red squares) from cells of ***A*** and ***B***. Data have been fitted with exponential saturation function (Eq. 1), with values for r_{max} and k of 15.4 pA and 0.024 photons^{-1} μm^2 (WT) and 23.0 pA and 0.078 photons^{-1} μm^2 ($PDEA^{D167A/D167A}$). Dashed lines indicate the half-saturating response intensities for both cell types. ***D***, Mean and SEM of single-photon responses of WT (black, $n = 7$) and $PDEA^{D167A/D167A}$ (red, $n = 10$). The waveform of the single-photon response was calculated for each cell from the squared mean and variance (Chen et al., 2000), and these waveforms were then averaged and plotted with SEM values for WT and $PDEA^{D167A/D167A}$ rods as functions of time. Note the much greater variability for the $PDEA^{D167A/D167A}$ rods.

In Figure 4*C*, we show response-intensity curves for the cells of Figure 4*A*, *B*. The data have been fit with a function of the form (Lamb et al., 1981) as follows:

$$r = r_{max}[1 - \exp(-k\phi)] \quad (1)$$

where r is the peak amplitude of the response, r_{max} is the maximum value of r in bright light, ϕ is the number of photons per μm^2 of the stimulus, and k is a constant with units of ϕ^{-1} (photons^{-1} μm^2). The dashed lines indicate the value of ϕ required to produce a half-maximal response in both kinds of receptors, which can be calculated from the values of the constant k in Equation 1. They are 29 photons μm^{-2} for WT rods and 8.9 photons μm^{-2} for $PDEA^{D167A/D167A}$ rods. By this measure, the $PDEA^{D167A/D167A}$ rods are ~3-fold more sensitive than WT rods.

We also estimated the sensitivity difference by stimulating the rods with a series of dim flashes of the same intensity and calculating the single-photon response from the squared mean and variance (Chen et al., 2000). We did this calculation for 7 WT rods and 10 $PDEA^{D167A/D167A}$ rods, and the results were then averaged point by point as a function of time and plotted with SEMs in Figure 4*D*. The peak amplitudes of the responses were 0.037 ± 0.004 for WT rods and 0.087 ± 0.016 for $PDEA^{D167A/D167A}$ rods. The $PDEA^{D167A/D167A}$ rods were thus between 2 and 3 times more sensitive than WT rods by this measure, roughly consistent with the results in Figure 4*A*–*C*.

Variability of single-photon response

The much greater values of the SEMs in Figure 4*D* for $PDEA^{D167A/D167A}$ rods seemed to indicate that cell-to-cell variation in the waveform and peak amplitude of the calculated single-photon response may be larger for the mutant rods than for WT. It is possible that this difference reflects changes in the transduction mechanism from cell to cell, caused, for example, by differences in PDE expression. It may however indicate, at least in part, some intrinsic variability in the single-photon response within the rod itself. Because previous model calculations had predicted an increase in intrinsic single-photon response variance with decreasing PDE expression (Reingruber et al., 2013, their Fig. 5*E*,*F*), we examined intrinsic variability by stimulating the rods with a light so dim that the majority of the responses were produced by single-photon absorptions.

In Figure 5*A*, *B*, we show representative responses from a WT rod and a $PDEA^{D167A/D167A}$ rod to a continuous series of 25 dim flashes of (on average) 2 photons μm^{-2}. The distribution of the number of Rh* produced by the flashes was calculated from the following Poisson equation:

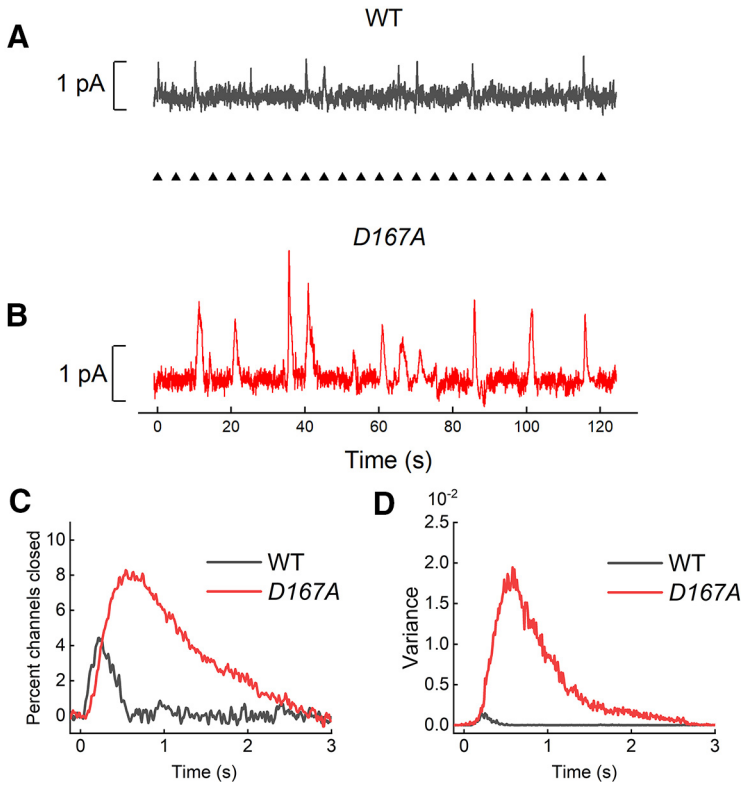

Figure 5. Responses from WT and $PDEA^{D167A/D167A}$ rods to a continuous series of 25 flashes (arrowheads) bleaching on average 0.6 Rh* per rod. ***A***, WT. ***B***, $PDEA^{D167A/D167A}$. Responses are representative of between 100 and 200 flashes given to each of 7 WT rods and 6 $PDEA^{D167A/D167A}$ rods. ***C***, ***D***, Nulls were excluded, and actual responses were collected from 7 WT rods and 6 $PDEA^{D167A/D167A}$ rods and normalized cell by cell to the maximum amplitude of the rod from which the recording was made. The normalized responses from all the rods were then used to compute point by point the mean (***C***) and variance (***D***) of the waveforms.

$$P_k = \frac{\lambda^k e^{-\lambda}}{k!} \qquad (2)$$

where P_k is the probability that k rhodopsins are activated by the flash, and λ is the mean number of activated rhodopsins. From the fraction of nulls and the value of P_0, we have estimated λ as ~0.6 Rh* (see Materials and Methods); and from this value and Equation 2, we calculate that for the responses of Figure 5*A*, *B*, on average 55% should be nulls, 33% should be single-photon responses, and 12% should be responses to 2 or more photons. Of those flashes that were not nulls and gave a response, 33 of 45 or 73% should be single-photon responses, with the remaining 27% resulting from 2 or more Rh*.

The results in Figure 5*A*, *B* show that a $PDEA^{D167A/D167A}$ rod gave responses that were much more variable than a WT rod; and because about three-fourths of the responses in both Figure 5*A* and Figure 5*B* will have been to single photons, we can conclude that single-photon responses in $PDEA^{D167A/D167A}$ rods are much more variable. To provide a quantitative estimate of this difference, we would ideally like to isolate only those responses that we could be sure were generated by single photons and calculate their mean and variance. Since, however, the responses of $PDEA^{D167A/D167A}$ rods were so variable, separation of single-photon responses from those produced by 2 or more photons could not be done with any confidence. We therefore proceeded in the following way. We first excluded the nulls and normalized all of the actual responses for each rod to the maximum response amplitude of that rod to a saturating light flash. We then calculated the means and variances of the normalized responses from all of the WT and $PDEA^{D167A/D167A}$ rods from which recordings like those in Figure 5*A*, *B* were made. These waveforms should mostly reflect the properties of responses to single photons.

The results of these calculations are given in Figure 5*C* (for means) and Figure 5*D* (for variances). Although the waveforms for the means in Figure 5*C* resemble those in Figure 4*D* for single-photon responses calculated from the squared-mean and variance, the calculations in Figure 4*D* assume that the variance of the *D167A* response is primarily the result of Poisson variability in the number of single-photon absorptions and not in variability in the single-photon amplitude, which the results in Figure 5*B* show to be quite large. As a result, the calculations in Figure 4*D* do not provide an accurate measure of the *D167A* single-photon response or of its SEM. This difficulty may explain the difference in the peak amplitude of the responses in these two figures, which is larger in Figure 4*D* than in Figure 5*C*, although the mean response in Figure 5*C* should have included a proportion of responses to 2 or more Rh*.

We measured the latency of the responses by fitting a third-order polynomial curve from the baseline to the peak of the response. We used the interval from the beginning of the light flash to the time when the response reached 5% of its maximum as the value for onset latency. No correction was made for the delay resulting in low-pass filtering of the responses. The mean onset latencies for the rods of Figure 5*C* obtained by this method were 43 ± 0.2 ms for WT rods and 120 ± 2 ms for $PDEA^{D167A/D167A}$ rods. We then subtracted the onset latency from the time the response reached its peak value to give a time-to-peak duration. The mean values of time to peak were 170 ± 1 ms for WT rods and 450 ± 60 ms for $PDEA^{D167A/D167A}$ rods. Both onset latency and time to peak were significantly different between WT rods and $PDEA^{D167A/D167A}$ rods at the same level of $p = 0.004$.

We show the variances of the response amplitudes in Figure 5*D*. The variance of peak amplitude was much greater for $PDEA^{D167A/D167A}$ rods (0.018 ± 0.003) than for WT rods (0.0014 ± 0.0005). These values were significantly different ($p = 0.02$). We calculated 95% confidence intervals for the variances of peak amplitude of both WT and $PDEA^{D167A/D167A}$ rods with bootstrap in MATLAB. These were 0.00073 – 0.0014 – 0.0025 for WT, and 0.013 – 0.018 – 0.022 for $PDEA^{D167A/D167A}$ (lower – mean – upper). The distributions for the two kinds of rods were nonoverlapping. We conclude that most of the difference in variance reflects a difference in the variance of the single-photon responses of individual rods rather than rod-to-rod differences, as also seems apparent from the results in Figure 5*A*, *B*.

The variances for latencies were even more discrepant. For onset latency, the variances were 120 ± 76 ms^2 for WT and 23,000 ± 3000 ms^2 for $PDEA^{D167A/D167A}$ rods ($p = 0.01$); and for time to peak, 460 ± 110 ms^2 for WT, and 75,000 ± 6500 ms^2 for $PDEA^{D167A/D167A}$ rods ($p = 0.005$). For both measures, the mean values of latency variances of the $PDEA^{D167A/D167A}$ rods were over 100-fold greater than for WT rods.

Response variability as a function of the brightness of the flash

To investigate the dependence of variability on the brightness of the flash, we made suction-electrode recordings from WT and $PDEA^{D167A/D167A}$ rods for increasing numbers of mean rhodopsins bleached per flash. These results are given in Figure 6 from representative recordings at three light levels. Responses to dim light were quite variable in latency and amplitude for the $PDEA^{D167A/D167A}$ rods, but this variability decreased as the stimuli were made brighter.

Variances were then calculated as a function of time in both WT (Fig. 7*A*) and $PDEA^{D167A/D167A}$ rods (Fig. 7*B*). For dim flashes, there was much more variance in the flash-to-flash responses of the mutant photoreceptors, which gradually decreased as the stimuli were made brighter. We then normalized the responses of each cell to the total dark current of that cell and measured the variance of the normalized peak-response amplitude. In Figure 7*C*, we have plotted individual data points as well as the average for all cells (stars). There is a significant difference in variance between WT and mutant photoreceptors for all three of the dimmer flashes ($p = 0.03$, 0.01, and 0.02) but not for the brightest light, where the mean variances were nearly identical (WT, 0.0014 ± 0.0007; $PDEA^{D167A/D167A}$, 0.0013 ± 0.0004).

In Figure 7*D*, *E*, we show variances for onset latency and time to peak, calculated as above for the single-photon responses. The variances of the $PDEA^{D167A/D167A}$ rods were consistently larger than the variances of the WT rods for the dimmer flashes, although not for the brightest flash which nearly saturated the rod. We conclude that, in addition to the amplitude, the shape of the waveform was much more variable for the mutant photoreceptors.

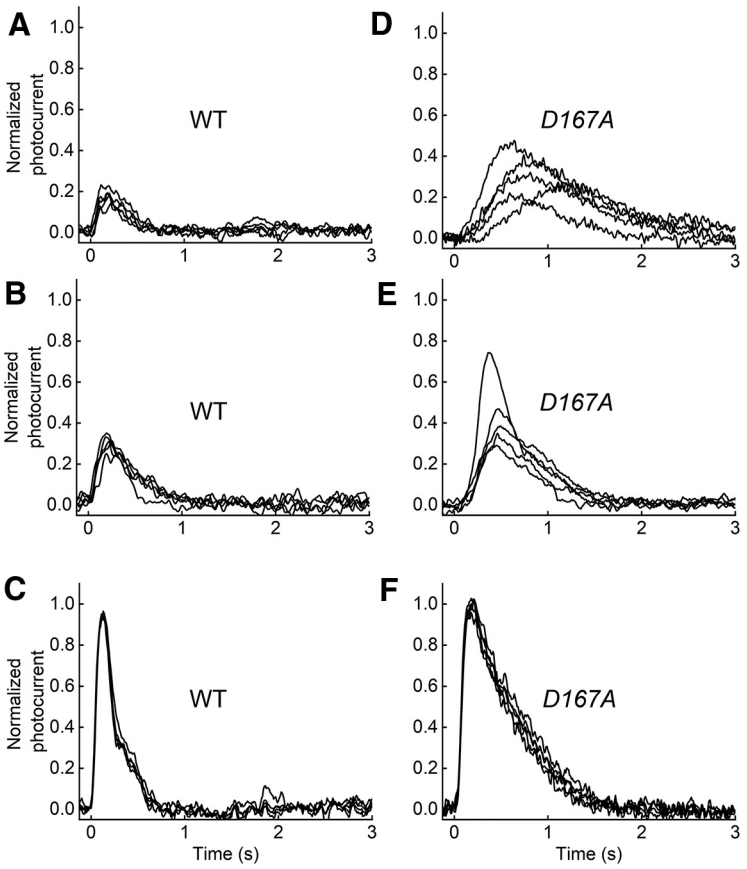

Figure 6. Dependence of variability on the brightness of the stimuli. Responses of representative WT rod (***A–C***) and $PDEA^{D167A/D167A}$ rod (***D–F***) for flashes bleaching on average 1.5 (***A***,***D***), 3.3 (***B***,***E***), and 31.5 (***C***,***F***) Rh*.

Discussion

In an attempt to investigate the function of noncatalytic cGMP binding in rod PDE modulation, we removed a key aspartate in the GAF A domain of PDEA. We discovered that the resulting $PDEA^{D167A/D167A}$ rods produced <1% of PDEA (Fig. 1*C*), probably because of the importance of the GAF A domain in PDE protein folding (Heikaus et al., 2009; Cote et al., 2021). Expression of PDEB was also depressed, as has been previously observed for other mouse mutations of the *PDEA* gene (Sakamoto et al., 2009), but the specific activities of the basal and trypsin-activated remaining enzyme were comparable with those of normal rod PDE (Fig. 2). Rods degenerated slowly, with more than half of the photoreceptors still present in 6-month-old mice (Fig. 3). Moreover, the $PDEA^{D167A/D167A}$ rods had light responses nearly twice as large as WT rods, probably from the decrease in basal PDE activity and a resulting increase in dark current (Fig. 4). Responses decayed slowly and were more variable in amplitude and waveform than WT rods. This variability was particularly marked for single-photon responses (Fig. 5) and may have resulted again from a decrease in spontaneous PDE activity, which produced temporal and spatial inhomogeneity in the dark cGMP concentration within the outer segment. Response variance diminished as flashes were made brighter, presumably from greater spatial uniformity of transduction in brighter light and eventual response saturation (Figs. 6 and 7). These experiments show that the concentration of PDE within the outer segment is critical for ensuring light responses of uniform amplitude and waveform by maintaining sufficient basal PDE activity, to ensure spatial and temporal continuity of dark cGMP concentration within the outer segment.

PDE expression and activity in $PDEA^{D167A/D167A}$ rods

Our experiments demonstrate a marked asymmetry in the function of the two rod PDE catalytic subunits. The presence of PDEB is a necessary requirement for functional enzyme, since a nonsense mutation in the gene for PDEB in *rd1* mice causes rapid and complete degeneration of the rods (Bowes et al., 1990). In contrast, the nearly complete absence of PDEA in $PDEA^{D167A/D167A}$ rods has a much milder effect, with degeneration proceeding much more slowly. The rods are apparently able to function for an extended period with almost no PDEA, but they survive no longer than 1-2 weeks if PDEB is absent.

It is likely that PDE activity in $PDEA^{D167A/D167A}$ rods is produced largely, if not exclusively, by PDEB as dimers rather than monomers. This is because of the importance of the dimeric structure for PDE stability and function (see, e.g., Gulati et al., 2019). Cones are known to have dimeric PDE formed from only a single kind of catalytic subunit (PDEC) (see Cote, 2021), and both rods and cones in lamprey express only one (and the same) catalytic subunit (Muradov et al., 2007). Moreover, the retina of the chicken seems not to express a PDEA, so its rod PDE is

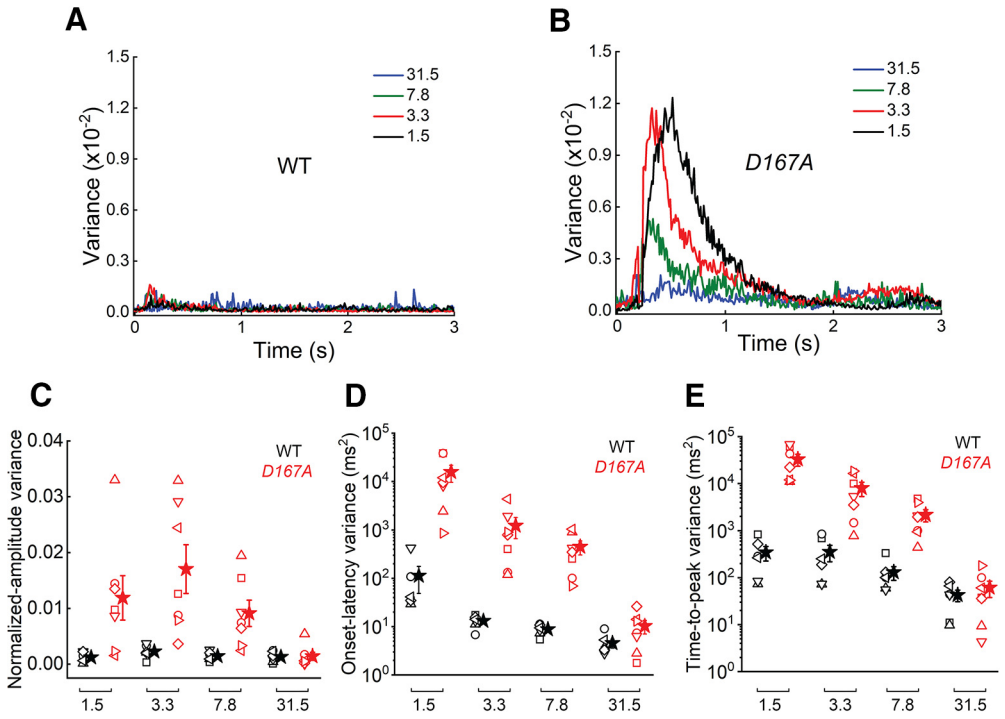

Figure 7. Response variance of $PDEA^{D167A/D167A}$ and WT rods. Total variance of each cell was calculated as a function of time in rods of (***A***) WT ($n = 6$) and (***B***) $PDEA^{D167A/D167A}$ ($n = 7$) with the same protocol as for Figure 6. ***C–E***, Variance of same WT rods (black) and $PDEA^{D167A/D167A}$ rods (red) for normalized amplitude (***C***), onset latency (***D***), and time to peak (***E***). Stimuli (in Rh*) are as indicated by brackets below each set of data points. Data points give value for each rod, with mean and SEM indicated by stars with bars.

apparently made up exclusively from PDEB (Huang et al., 2004). This observation also supports the functionality of a PDEB dimer in $PDEA^{D167A/D167A}$ rods.

Response amplitude, waveform, and variability of $PDEA^{D167A/D167A}$ rods

The dark current of $PDEA^{D167A/D167A}$ rods is about twice as large as that of WT rods (Fig. 4*A–C*). Because the open probability of the cGMP channel of the rod outer segment varies monotonically with the cGMP concentration (see, e.g., Zagotta and Siegelbaum, 1996), this increase in dark current indicates that the free-cGMP concentration of the outer segment is larger than in a WT rod, probably from reduced basal cGMP hydrolysis. And since the concentration of outer-segment Ca^{2+} also varies with the value of the steady-state current (Matthews and Fain, 2003), $PDEA^{D167A/D167A}$ rods would be expected to have an increased outer-segment free-Ca^{2+} concentration and a reduced activity of cGMP cyclase. These changes will produce a decrease in the rate constant of hydrolysis of PDE (β_D) and of the rate of turnover of cGMP in darkness. As a result, the response of the $PDEA^{D167A/D167A}$ rod does not rapidly decay like the WT response but continues to rise, reaching a larger peak amplitude at a later time. Although most of the change in waveform can be attributed to the change in β_D (A. Abtout and J. Reingruber, unpublished observations), there is an initial delay in the $PDEA^{D167A/D167A}$ response which may be caused by a decrease in the rate of activation of PDE, perhaps because of longer seek times by transducin. There may also be additional, more subtle differences in enzyme function, which may explain the small alteration we observed in limiting time constant.

The most striking difference in $PDEA^{D167A/D167A}$ rods is the marked increase in response variability compared with WT rods, especially for single-photon responses and dim flashes (Figs. 5-7). Reingruber et al. (2013) estimated that, in a dark-adapted mouse rod, there is on average one spontaneously active PDE per outer-segment compartment formed by the spaces between disks. In a $PDEA^{D167A/D167A}$ rod, there would be on average only 1 per 10-20 disks, if we assume that the number of spontaneously active molecules is proportional to the enzyme expression level. Such a low basal activity would of necessity produce spatial and temporal differences in cGMP concentration in different compartments of the outer segment. The effect of a single photon would then depend on the place in the outer segment where the photon was absorbed by rhodopsin, producing increased variance in response amplitude and waveform in dim light. A decrease in the level of expression of PDE would also increase the level of free Ca^{2+} in the outer segment, which could alter several of the reactions in the transduction cascade, including the phosphorylation of rhodopsin (Kawamura, 1993; Whitlock and Lamb, 1999), the activity of guanylyl cyclase (Koch and Stryer, 1988; Gross et al., 2012), and the functioning of the PDE enzyme itself (Fain, 2011). A clear understanding of the effects of all of these mechanisms on response variability may emerge from model calculations of the effect of reducing PDE expression on all of the functional properties of the rod (A. Abtout, K. G. Griffis, A. Morshedian, G. L. Fain, and J. Reingruber, unpublished observations).

PDE and the sensitivity of vision

When Baylor et al. (1979) made the first recordings of single-photon responses, they noted a surprising uniformity in response amplitude and waveform. Several theories have been proposed for this phenomenon, including deactivation of rhodopsin (Rieke and Baylor, 1998; Whitlock and Lamb, 1999; Field and Rieke, 2002; Hamer et al., 2003; Doan et al., 2006) and rapid Ca^{2+}-dependent feedback from guanylyl cyclase (Gross et al., 2012). Our experiments show that, in addition to features of response decay, the reproducibility of the response depends

critically on the level of expression and basal activity of the PDE effector enzyme.

The expression of PDE in the rod seems to be under selection pressure to ensure that spontaneous PDE activity is fixed at a sufficiently high level. It is significant that the large rods of salamander and the much smaller rods of WT mice have nearly the same average PDE basal activity with, for both species, about one spontaneously active PDE molecule per compartment (see Reingruber et al., 2013). This number could remain the same in the smaller outer segments of mouse only if the expression level of PDE were several-fold greater than in amphibians, as seems indeed to be the case (see Pugh and Lamb, 2000).

Insect photoreceptors generate single-photon responses of remarkable variability in time course and amplitude (see Hardie and Postma, 2008). Why are vertebrate rod responses so much less variable? The constancy of the single-photon response in vertebrates may be required for reliable transmission across the rod-bipolar synapse (Kojima et al., 2000; Sampath and Rieke, 2004; Okawa et al., 2010), or to facilitate temporal resolution of visual signals in dim light (Rieke and Baylor, 1998; Field et al., 2019). Experiments are in progress to test these possibilities by comparing signal transmission to bipolar cells from WT rods and rods with diminished PDE expression, such as PDE heterozygotes (Majumder et al., 2015) and $PDEA^{D167A/D167A}$ rods. It may also be interesting to compare responses of ganglion cells and, ultimately, visual behavior in animals with different levels of PDE expression. These experiments may help us understand the functional significance of the remarkable reproducibility of the single-photon response in vertebrate vision.

References

Abtout A, Fain G, Reingruber J (2021) Analysis of waveform and amplitude of mouse rod and cone flash responses. J Physiol 599:3295–3312.

Arshavsky VY, Burns ME (2012) Photoreceptor signaling: supporting vision across a wide range of light intensities. J Biol Chem 287:1620–1626.

Baehr W, Devlin MJ, Applebury ML (1979) Isolation and characterization of cGMP phosphodiesterase from bovine rod outer segments. J Biol Chem 254:11669–11677.

Baylor DA, Lamb TD, Yau KW (1979) Responses of retinal rods to single photons. J Physiol 288:613–634.

Bowes C, Li T, Danciger M, Baxter LC, Applebury ML, Farber DB (1990) Retinal degeneration in the rd mouse is caused by a defect in the beta subunit of rod cGMP-phosphodiesterase. Nature 347:677–680.

Burns ME, Pugh EN Jr (2010) Lessons from photoreceptors: turning off G-protein signaling in living cells. Physiology (Bethesda) 25:72–84.

Calvert PD, Ho TW, LeFebvre YM, Arshavsky VY (1998) Onset of feedback reactions underlying vertebrate rod photoreceptor light adaptation. J Gen Physiol 111:39–51.

Chen CK, Burns ME, He W, Wensel TG, Baylor DA, Simon MI (2000) Slowed recovery of rod photoresponse in mice lacking the GTPase accelerating protein RGS9-1. Nature 403:557–560.

Cote RH (2021) Photoreceptor phosphodiesterase (PDE6): activation and inactivation mechanisms during visual transduction in rods and cones. Pflugers Arch 473:1377–1391.

Cote RH, Bownds MD, Arshavsky VY (1994) cGMP binding sites on photoreceptor phosphodiesterase: role in feedback regulation of visual transduction. Proc Natl Acad Sci USA 91:4845–4849.

Cote RH, Gupta R, Irwin MJ, Wang X (2021) Photoreceptor phosphodiesterase (PDE6): structure, regulatory mechanisms, and implications for treatment of retinal diseases. Adv Exp Med Biol. Advance online publication. Retrieved Jun 26, 2021. doi:10.1007/5584_2021_649.

Doan T, Mendez A, Detwiler PB, Chen J, Rieke F (2006) Multiple phosphorylation sites confer reproducibility of the rod's single-photon responses. Science 313:530–533.

Fain GL (2011) Adaptation of mammalian photoreceptors to background light: putative role for direct modulation of phosphodiesterase. Mol Neurobiol 44:374–382.

Fain GL (2019) Sensory transduction, 2nd edition. Oxford: Oxford University Press.

Field GD, Rieke F (2002) Nonlinear signal transfer from mouse rods to bipolar cells and implications for visual sensitivity. Neuron 34:773–785.

Field GD, Uzzell V, Chichilnisky EJ, Rieke F (2019) Temporal resolution of single-photon responses in primate rod photoreceptors and limits imposed by cellular noise. J Neurophysiol 121:255–268.

Gross OP, Pugh EN Jr, Burns ME (2012) Calcium feedback to cGMP synthesis strongly attenuates single-photon responses driven by long rhodopsin lifetimes. Neuron 76:370–382.

Gulati S, Palczewski K (2021) New focus on regulation of the rod photoreceptor phosphodiesterase. Curr Opin Struct Biol 69:99–107.

Gulati S, Palczewski K, Engel A, Stahlberg H, Kovacik L (2019) Cryo-EM structure of phosphodiesterase 6 reveals insights into the allosteric regulation of type I phosphodiesterases. Sci Adv 5:eaav4322.

Hamer RD, Nicholas SC, Tranchina D, Liebman PA, Lamb TD (2003) Multiple steps of phosphorylation of activated rhodopsin can account for the reproducibility of vertebrate rod single-photon responses. J Gen Physiol 122:419–444.

Hardie RC, Postma M (2008) Phototransduction in microvillar photoreceptors of *Drosophila* and other invertebrates. In: The senses: a comprehensive reference vision volume (Albright M, Basbaum K, Shepher W, eds), pp 77–130. Oxford: Academic.

Heikaus CC, Pandit J, Klevit RE (2009) Cyclic nucleotide binding GAF domains from phosphodiesterases: structural and mechanistic insights. Structure 17:1551–1557.

Huang D, Hinds TR, Martinez SE, Doneanu C, Beavo JA (2004) Molecular determinants of cGMP binding to chicken cone photoreceptor phosphodiesterase. J Biol Chem 279:48143–48151.

Kawamura S (1993) Rhodopsin phosphorylation as a mechanism of cyclic GMP phosphodiesterase regulation by S-modulin. Nature 362:855–857.

Koch KW, Stryer L (1988) Highly cooperative feedback control of retinal rod guanylate cyclase by calcium ions. Nature 334:64–66.

Kojima D, Mano H, Fukada Y (2000) Vertebrate ancient-long opsin: a green-sensitive photoreceptive molecule present in zebrafish deep brain and retinal horizontal cells. J Neurosci 20:2845–2851.

Lamb TD, McNaughton PA, Yau KW (1981) Spatial spread of activation and background desensitization in toad rod outer segments. J Physiol 319:463–496.

Majumder A, Pahlberg J, Muradov H, Boyd KK, Sampath AP, Artemyev NO (2015) Exchange of cone for rod phosphodiesterase 6 catalytic subunits in rod photoreceptors mimics in part features of light adaptation. J Neurosci 35:9225–9235.

Matthews HR, Fain GL (2003) The effect of light on outer segment calcium in salamander rods. J Physiol 552:763–776.

Muradov H, Boyd KK, Artemyev NO (2004) Structural determinants of the PDE6 GAF A domain for binding the inhibitory gamma-subunit and noncatalytic cGMP. Vision Res 44:2437–2444.

Muradov H, Boyd KK, Kerov V, Artemyev NO (2007) PDE6 in lamprey *Petromyzon marinus*: implications for the evolution of the visual effector in vertebrates. Biochemistry 46:9992–10000.

Nymark S, Frederiksen R, Woodruff ML, Cornwall MC, Fain GL (2012) Bleaching of mouse rods: microspectrophotometry and suction-electrode recording. J Physiol 590:2353–2364.

Okawa H, Miyagishima KJ, Arman AC, Hurley JB, Field GD, Sampath AP (2010) Optimal processing of photoreceptor signals is required to maximize behavioural sensitivity. J Physiol 588:1947–1960.

Pugh EN Jr, Lamb TD (2000) Phototransduction in vertebrate rods and cones: molecular mechanism of amplification, recovery and light adaptation. In: Handbook of biological physics: molecular mechanisms of visual transduction (Stavenga DG, DeGrip WJ, Pugh EN, Jr, eds), pp 183–255. Amsterdam: Elsevier.

Reingruber J, Pahlberg J, Woodruff ML, Sampath AP, Fain GL, Holcman D (2013) Detection of single photons by toad and mouse rods. Proc Natl Acad Sci USA 110:19378–19383.

Reingruber J, Holcman D, Fain GL (2015) How rods respond to single photons: key adaptations of a G-protein cascade that enable vision at the physical limit of perception. Bioessays 37:1243–1252.

Rieke F, Baylor DA (1998) Origin of reproducibility in the responses of retinal rods to single photons. Biophys J 75:1836–1857.

Sakamoto K, McCluskey M, Wensel TG, Naggert JK, Nishina PM (2009) New mouse models for recessive retinitis pigmentosa caused by mutations in the Pde6a gene. Hum Mol Genet 18:178–192.

Sampath AP, Rieke F (2004) Selective transmission of single photon responses by saturation at the rod-to-rod bipolar synapse. Neuron 41:431–443.

Sothilingam V, Garcia Garrido M, Jiao K, Buena-Atienza E, Sahaboglu A, Trifunovic D, Balendran S, Koepfli T, Muhlfriedel R, Schon C, Biel M, Heckmann A, Beck SC, Michalakis S, Wissinger B, Seeliger MW, Paquet-Durand F (2015) Retinitis pigmentosa: impact of different Pde6a point mutations on the disease phenotype. Hum Mol Genet 24:5486–5499.

Wang L, Shao Y, Guan Y, Li L, Wu L, Chen F, Liu M, Chen H, Ma Y, Ma X, Liu M, Li D (2015) Large genomic fragment deletion and functional gene cassette knock-in via Cas9 protein mediated genome editing in one-cell rodent embryos. Sci Rep 5:17517.

Whitlock GG, Lamb TD (1999) Variability in the time course of single photon responses from toad rods: termination of rhodopsin's activity. Neuron 23:337–351.

Zagotta WN, Siegelbaum SA (1996) Structure and function of cyclic nucleotide-gated channels. Annu Rev Neurosci 19:235–263.